

The Effect of Fiber Diameter on the Compressive Strength of Composites - A 3D Finite Element Based Study

Chandra S. Yerramalli¹ and Anthony M. Waas²

Abstract: Results from a 3D finite element based study of the compression response of unidirectional fiber reinforced polymer matrix composites (FRPC) are presented in this paper. The micromechanics based study was used to simulate the compressive response of glass and carbon fiber reinforced polymer matrix composites, with a view to understanding the effect of fiber diameter on compression strength. Results from the modeling and simulation indicate the presence of a complex three dimensional stress state in the matrix of the FRPC. Results from the simulation highlight the role of fiber diameter on the compressive response of FRPC. In particular, it is shown that, depending on the fiber diameter, fiber breaking may precede the attainment of a limit load due to fiber misalignment, thus, precipitating a different mechanism for the initiation of kink bands.

keyword: compression, finite element, size effects, composites, kinking, failure mechanisms

1 Introduction

Experimental and analytical models presented in the literature indicate the complexity and the difficulty in modeling the unidirectional fiber composite compressive response and failure accurately. Several previous experimental studies and associated analytical modeling have established kink banding as a dominant mode of compressive failure in high fiber volume fraction FRPC, [Waas and Schultheisz (1996)]. The increase in available computational power and the recent advances in numerical modeling of instability problems [Pichler and Mang (2000) and Iura and Atluri (2003)], provide a means to understand this problem in a true 3D setting. In this

study, a 3D finite element micro-mechanics model of a FRPC is presented and used to understand the compressive response and failure of FRPC. In doing so, an attempt is made to understand 3D effects in the kinking failure process, and to delineate the role of finite bending stiffness and its influence on the mechanism of kink banding.

Previous analytical and numerical attempts to analyze the kinking failure mechanism are two dimensional, based on a model of the composite that assumes it to be a two constituent alternately layered medium under plane strain conditions. A comprehensive summary of the literature on modeling upto 1999 is contained in the papers by [Waas and Schultheisz (1996), Fleck (1997), and Naik and Kumar (1999)]. Beyond this time, investigations related to compressive response of FRPC have been reported by [Lee and Waas (1999), Jensen (1999), Vogler, Hsu, and Kyriakides (2000, 2001), Vogler and Kyriakides (1999, 2001), and, Niu and Talreja (2000)].

Among previous studies, [Vogler, Hsu, and Kyriakides (2000)], modeled the composite as a 3D plate, but the fibers were assumed to be periodic in the third dimension and hence only a 2D slice of the composite was considered. In a composite cylindrical specimen like that considered here, the fibers are arranged in a random fashion and the three dimensionality of the random arrangement of fibers in a cylinder cannot be modeled in a 2D manner. It can be argued that a 2D model of FRPC captures the appropriate mechanics at large fiber volume fractions, however, a 3D model is most appropriate to capture two important effects of FRPC compressive behavior. These are the influence of the complex 3D shear state that develops in the sandwiched matrix between the fibers in the region where kink bands (deformation localization) develop, and, the effect of finite fiber bending stiffness on the mechanism of kink band initiation and formation. In addition to these two effects, there is experimental evidence and characterization of carbon fiber as

¹ Ph.D student, University of Michigan, currently, Postdoctoral Research Fellow, McKay Orthopaedic Research Labs, University of Pennsylvania.

² Professor, Aerospace Engineering Department, University of Michigan, author to whom all correspondence should be addressed. (dcw@umich.edu, Tel: 734-764-8227, Fax: 734-763-0578)

a orthotropic solid, [Kawabata (1988)]. Yet, the effect of fiber orthotropy on compression response in a true 3D setting has not been investigated before.

The issues that are of particular interest in the current finite element study are as follows; (a) Comparison of the predicted compressive strength between a true 3D finite element model, a corresponding approximate 2D finite element model under pure compression, and, an available analytical prediction, (b) the effect of orthotropic fiber properties on the predicted maximum stress at a given angle of fiber misalignment, and (c) the dependency of the maximum stress on the fiber diameter. The resolution of the above issues would establish, among other things the dependency of critical kinking stress on the fiber diameter. It is to be noted that previous analytical models of kinking assume that the kink band is already developed, [Budiansky and Fleck (1993)]. Consequently, the effect of finite fiber bending stiffness and fiber orthotropy on the predicted compression strength associated with kinking failure is not accounted for. The effect of fiber diameter, which accounts for finite fiber bending stiffness, and fiber orthotropy are directly captured via a 3D micro-mechanics based finite element model, as has been presented in this paper.

2 Modeling

A unidirectional fiber reinforced composite cylinder was modeled using 8 noded reduced order brick elements, C3D8R, using the commercial finite element software, ABAQUS. Hourglass stiffness control was adopted to prevent the hourglassing of the brick elements. The composite cylinder geometry consisting of cylindrical fibers and matrix was meshed using the commercial meshing software HYPERMESH. Initially, a total of 37 fibers was included within a representative circular cylindrical microsection for both glass and carbon composite finite element models. An isometric view of the 3D finite element model is shown in figure 1. The carbon composite and glass composites were modeled for a fiber volume fraction of 0.5. In case of the glass composite finite element model, the fiber diameter was varied to study the effect of fiber diameter on the maximum stress. For this purpose the number of fibers in the models was kept the same. This resulted in two glass composite models with different composite outer radius, r_c . The cylinder length of both models were kept the same. 2D finite element models of carbon FRPC were used to predict the compressive

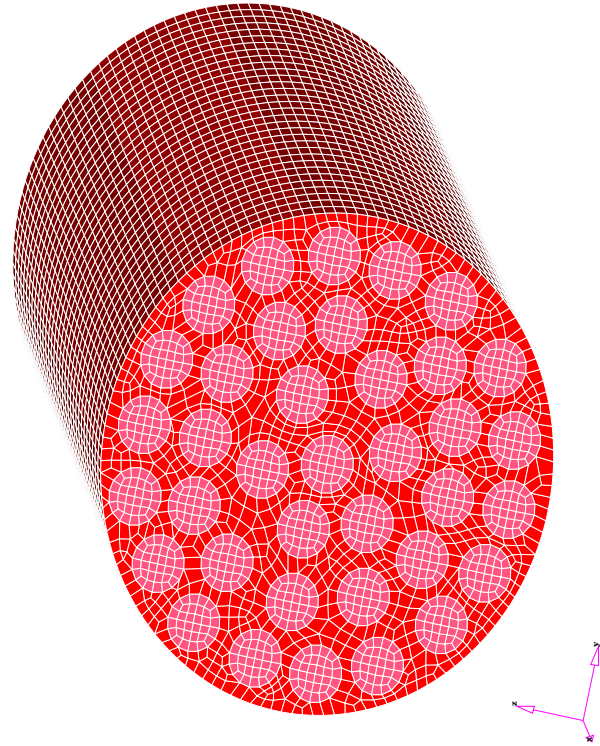


Figure 1 : A 3D finite element micro-mechanical model of a composite cylinder

sive strength of carbon FRPC with, $V_f = 0.5$, so that the 2D and 3D model predictions could be compared against each other and also against the analytical prediction of [Budiansky and Fleck (1993)]. Details of each of these models are given in Table 1. In case of carbon fiber, the effect of orthotropy of the carbon fiber on the predicted stress response was studied. The orthotropic properties of carbon fiber are obtained from [Lee and Waas (1999)] and are as follows, $E_{11} = 276000(MPa)$, $E_{22} = E_{33} = 8760(MPa)$, $G_{12} = G_{13} = 12000(MPa)$, $G_{23} = 3244(MPa)$, $\nu_{12} = 0.35$. In those cases where the carbon fiber is assumed isotropic, the material properties are given in Table 2. In section 3.2, results from a scaling study to determine size effects associated with the FE models are presented. For this purpose, two different types of scaling are introduced and discussed.

2.1 Initial Geometric Imperfection

An important consideration in studies related to compressive response of structures is the effect of initial geometric imperfection on the load-end shortening, $(P - \Delta)$

Model Name	Total Elements	Total Nodes	Length	Radius	Fiber radius	V_f
			$L (\mu m)$	$r_c (\mu m)$	$r_f (\mu m)$	
Carbon-1	64704	68673	64	21.5	2.5	0.5
Carbon-2D	10000	30349	710	250	2.5	0.5
Glass-1	64704	68673	306.43	58	6.75	0.5
Glass-2	64704	68673	306.43	103	12	0.5

Table 1 : 3D finite element model details

curve. In cases where the $P - \Delta$ curve shows a load maximum (limit load), it is of interest to determine the effect of imperfection magnitude on the load maximum. By doing so, one can generate a plot of maximum load against imperfection magnitude. From this plot, one can obtain the maximum load in the limit of vanishing imperfection magnitude (see figure 2).

	$E_f(\text{MPa})$	ν
Glass fiber	72000	0.22
Carbon fiber	276000	0.35
Vinylester	3585	0.36

Table 2 : Material properties of fiber and matrix

H_1	Mode-1	Mode-3
64	1.0334	0
32	0.5050	1.0179

Table 3 : Normalised displacements from buckling analysis of FE model(carbon-1)

For the purpose of generating an appropriate initial geometric imperfection shape, a linear buckling analysis of the models was performed and the buckling mode shapes (eigenmodes) were used to introduce the imperfection into the finite element models. As can be seen

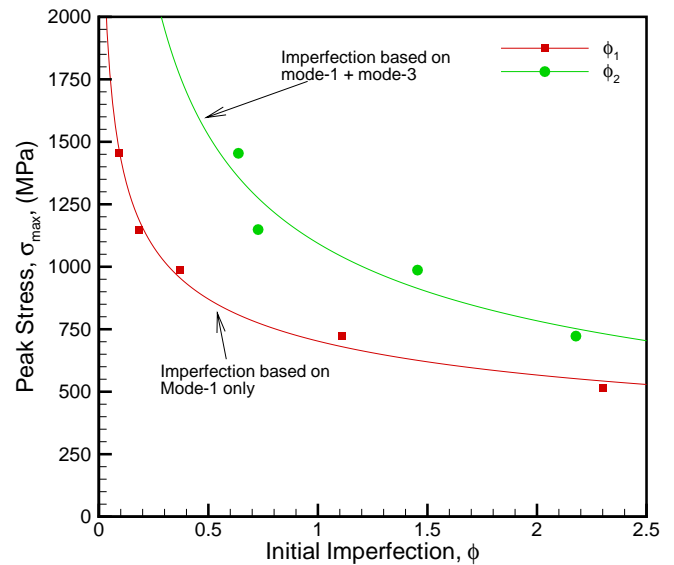


Figure 2 : Peak stress, σ_{max} as a function of initial imperfection, ϕ , to illustrate the different definitions of the initial misalignment angle

from figure 3 and figure 4, eigenmode-1 is a deformed cantilever mode and is a long wavelength imperfection mode. Whereas, eigenmode-3 shows a maximum lateral amplitude at the center of the cylinder. Thus, a combination of these two modes was used with varying amounts of magnitude to introduce a series of initial geometric imperfections in the composite. These imperfections lead to initial fiber misalignment that can be categorized through an initial fiber misalignment angle, (ϕ). The imperfection angle can be calculated based on the mode shapes chosen to perturb the original geometry. From the eigenmodes, the normalized displacement (U_1, U_2, U_3) for each mode can be obtained. Then, using the displacements in the 2 – 3 plane, (U_2, U_3), the

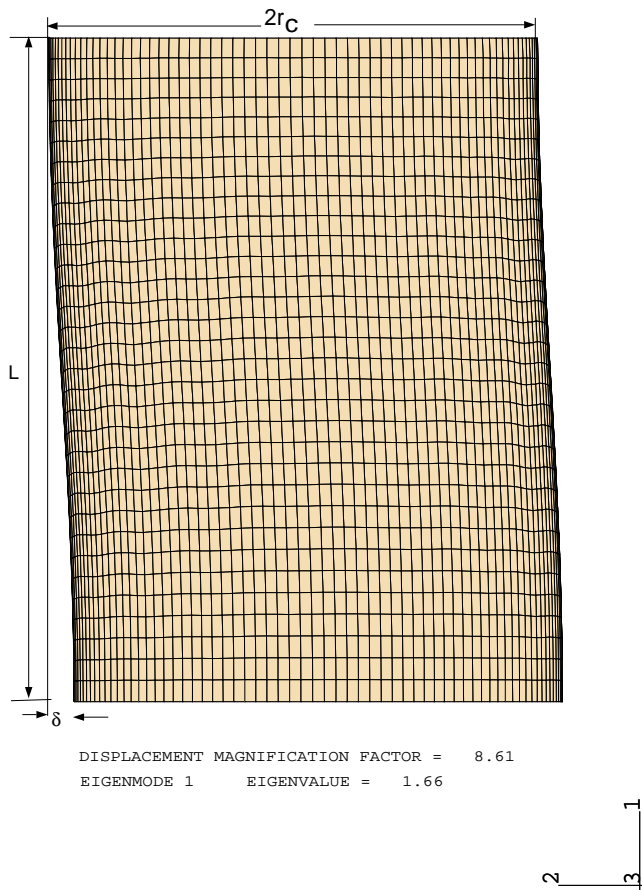


Figure 3 : Mode-1 displacement of 3D FE model

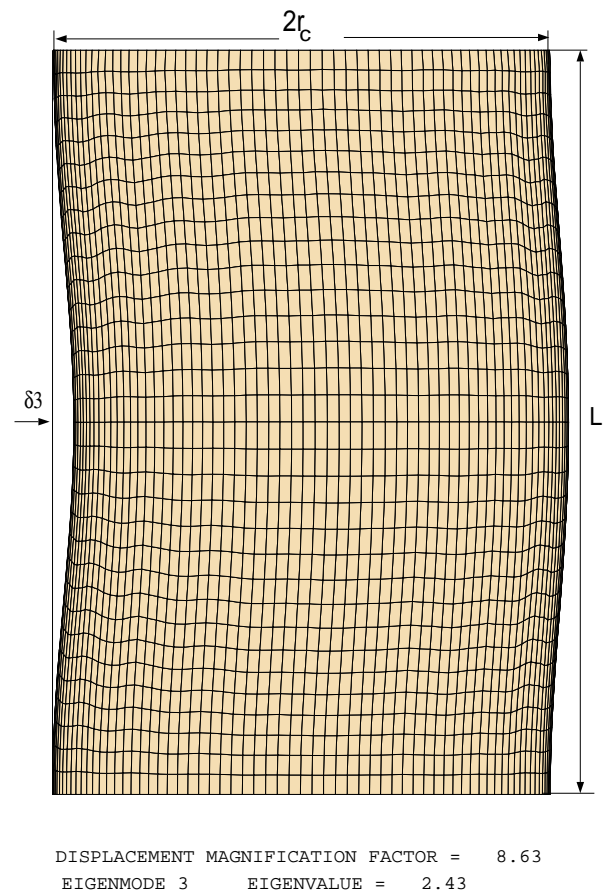


Figure 4 : Mode-3 displacement of 3D FE model

radius vector, r_d , by which the nodes are displaced in the 2 – 3 plane is calculated. Further, with a knowledge of the location of these nodes along the 1 direction (the fiber direction), the imperfection angle can be calculated. The maximum values of the radius vector, r_d , for different mode shapes and the location of these maximum values are given in Table 3. In case of using more than one mode shape to generate the initial imperfection (as has been done here with mode-1 and mode-3), the imperfection angle is calculated as follows. If δ_1 is the mode-1 radius vector and s_1 is the scaling factor, then the actual perturbation of the mesh, Δ_1 , would be $s_1 \times \delta_1$. Similarly, for mode-3, with s_3 as the scaling factor and δ_3 as the radius vector, then the actual perturbation of the mesh, Δ_3 , would be $s_3 \times \delta_3$. Thus, the total perturbation of the mesh, Δ_{tot} , would be a linear combination of these two perturbations given by $\Delta_1 + \Delta_3$. The imperfection angle, ϕ can be obtained from $\tan^{-1}(\Delta_{tot}/H1)$. The maximum value is taken as the imperfection angle of the mesh. However, it should be noted that the imperfection

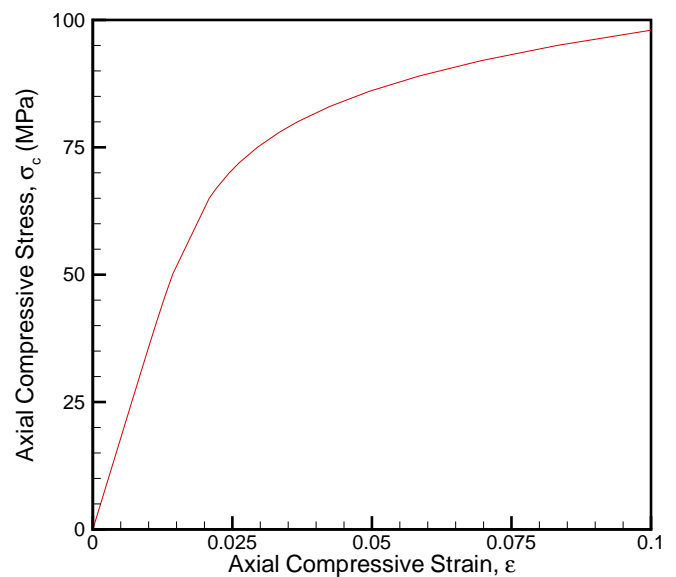


Figure 5 : Pure compression response of vinyl ester matrix used as input for FE modeling

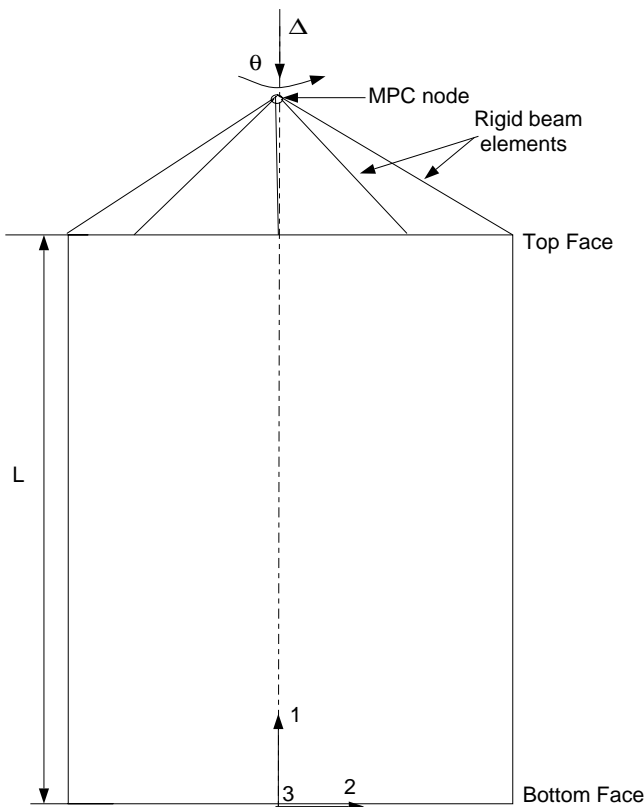


Figure 6 : A schematic of the FE model for pure compression and pure torsion

angle calculated is predicated on the basis that the mesh is being deformed in a homogeneous manner. As can be seen in figure 3 and figure 4, the displaced shape is non-homogeneous and thus the misalignment angle is a function of the axial position at which it is measured. The average initial fiber misalignment will be smaller than that based on the estimate $\tan^{-1}(\Delta_{tot}/H1)$. After the eigen mode-shapes are obtained from the finite element model, compressive response studies on the perturbed mesh are carried out in a setting that includes both, geometric and material non-linearity. For this purpose, the fibers are assumed to be linearly elastic isotropic or orthotropic as the case may be, the matrix is modeled as a J2 incremental theory of plasticity solid [Mendelson (1983)] and an arc-length tracing nonlinear solution process (RIKS method) is used to obtain the overall $P - \Delta$ curve of the micro-model. An arc-length procedure is needed to accommodate any ‘snap-back’ that can develop in the $P - \Delta$ response. The complete non-linear uni-axial stress-strain curve of the matrix that is used in the present study is shown in

figure 5. This non-linear curve is also the relation between the equivalent stress and equivalent strain for a J2 incremental theory plastic solid with a Von-Mises yield criterion and an associated flow rule [Mendelson (1983)].

2.2 Model Implementation

The straight fiber finite element models were perturbed using the procedure described in the preceding section to generate 3D perturbed finite element models of the composite with known initial geometric imperfections and then subjected to displacement control axial loading in a geometrically non-linear setting. Prior to conducting the axial compression studies, the response of the model to pure torsion loading was examined so that the shear stress-shear strain ($\tau - \gamma$) response of the FE model would match the ($\tau - \gamma$) response measured through experiment. To perform the torsion loading, a multi-point constraint option available in the ABAQUS software was used to constrain the motion of all the nodes on the top surface to move along the axial direction at the prescribed rate of displacement. The use of a MPC is useful in the torsion loading case since the rotation on the MPC node is translated into displacements along the tangential and radial directions for the face nodes. A schematic of the FE model along with the MPC node and the axis locations are shown in figure 6. The boundary conditions used for pure compression and pure torsion cases are shown in Table 4-5. For the loading cases studied, the models were allowed to ‘breathe’, i.e. the displacements along the 2 and 3 directions were free on both cylinder end faces.

The procedure used for studying the compressive response of the composites is as follows; first the 3D finite element models were used to generate the torsional response. The matrix non-linear properties were ‘calibrated’ to obtain the composite shear stress-shear strain ($\tau - \gamma$) response of the 3D FE model to be similar to the experimentally measured shear stress-shear strain curve. The model response was compared against the experimental shear stress-strain curve as shown in figure 7. The following is to be noted. The linear part of the $\tau - \gamma$ curve was found to match the linear part of the experimentally obtained $\tau - \gamma$ curve exactly. In order for the FE models $\tau - \gamma$ curve to match the experimental $\tau - \gamma$ curve in the non-linear regime, the non-linear (plastic) part of the $\sigma - \epsilon$ curve shown in figure 5 had to be changed. This is because, the present 3D FE model is a representative microsection (containing 37 fibers) of the

Node/face	U1	U2	U3	θ_1	θ_2	θ_3
MPC node	Δ	Free	Free	Free	Fixed	Fixed
Bottom	Fixed	Free	Free	-	-	-

Table 4 : Boundary conditions for pure compression

Node/face	U1	U2	U3	θ_1	θ_2	θ_3
MPC node	Fixed	Fixed	Fixed	θ	Fixed	Fixed
Bottom	Free	Fixed	Fixed	-	-	-

Table 5 : Boundary conditions for pure torsion

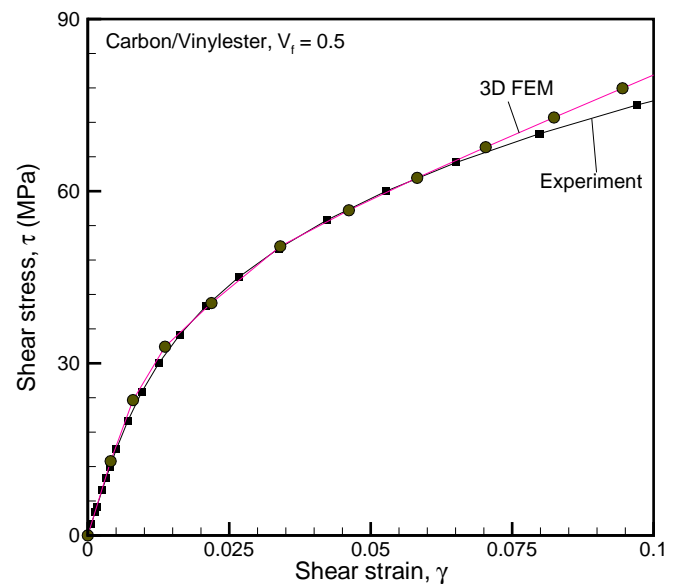
much larger laboratory specimen that contains approximately ‘125,000’ fibers within a radius of ‘3.35mm’ (see [Yerramalli (2003); Yerramalli and Waas (2003)], for details). For the purpose of studying compressive response, a numerical FE model of a representative micro-section is deemed equivalent to the actual laboratory specimen when both the FE model and the laboratory specimen contain the same fiber volume fraction and the same overall composite $\tau - \gamma$ response curve. After this ‘equivalence’ was established, the 3D models were used to generate compressive response curves. In section 3.2 of this paper, two different types of scaling related to interpreting finite element model results are presented and discussed.

3 Results

3.1 Comparison of 3D and 2D Model Predictions

The pure compressive response curves for a range of initial imperfection magnitudes are shown in figure 8. In the plot, σ_c is the macroscopic axial stress (axial load divided by the initial microsection cylinder crosssectional area) and ϵ_c is the macroscopic strain based on end-shortening (i.e. the axial end shortening divided by the initial microsection cylinder length). A note about the initial imperfection is in order. Recall, that two curves were shown in figure 2, which showed the dependency of maximum macroscopic stress on imperfection magnitude. In the first curve, the initial imperfection (misalignment angle) is based on the magnitude of the mode-1 imperfection

(even though, both mode-1 and mode-3 imperfections are included in the 3D FE model). This is because, as explained earlier, the misalignment angle is a function of axial position. Thus, for comparison purposes, it is clearer to define the geometric imperfection based on the mode-1 shape only. The misalignment angles indicated in Figure 8 are based on the definition that includes only the mode-1 imperfection, and this will be so for the remainder of this paper.

**Figure 7** : Comparison of the experimental and 3D FE shear stress-strain curve for a carbon/vinylester composite of $V_f = 0.5$

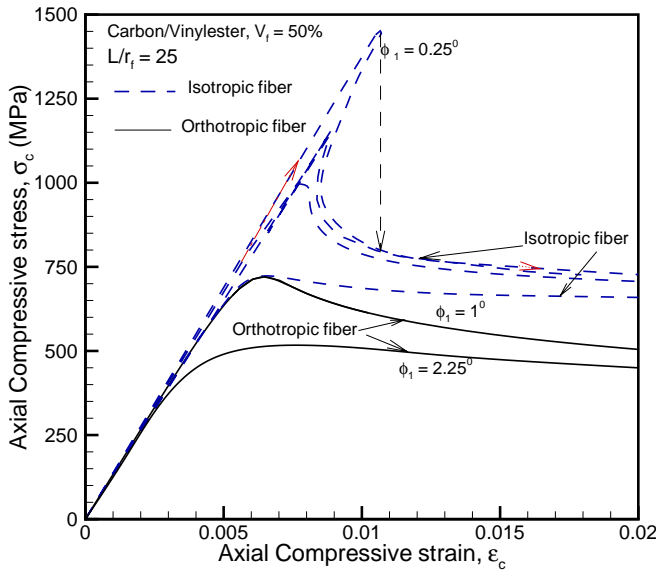


Figure 8 : Compressive response curves of carbon/vinylester composite of $V_f = 0.5$ for different values of imperfections

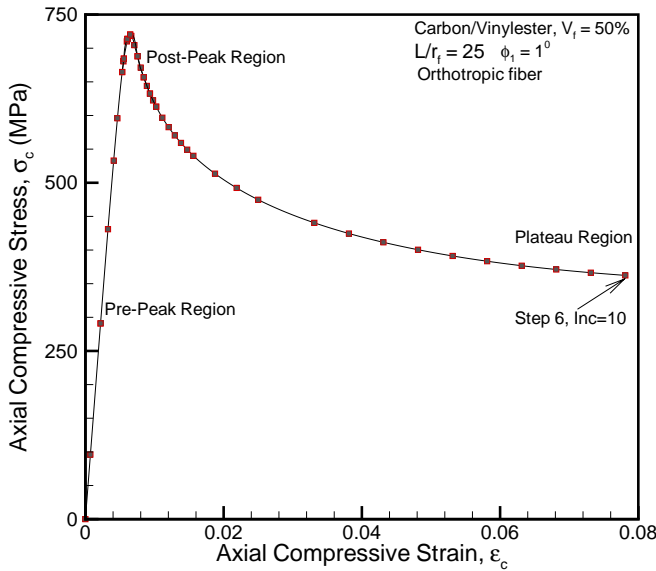


Figure 9 : Compressive response curve of carbon/vinylester composite of $V_f = 0.5$ and $\phi_1 = 1^\circ$ with orthotropic fiber properties

An explanation of a typical $\sigma - \epsilon$ curve as shown in figure 8 is in order. At first, the model behaves linearly. With continued loading (consider the $\phi_1 = 0.25^\circ$ case, for example), the matrix material in the region of initially misaligned fibers is subjected to increasing amounts of shear strain. This results in a progressively

decreasing shear stiffness of the matrix (inferred from the shear stress-shear strain curve of the composite, figure 7), which in turn, provides decreasing support to the fibers. A point is reached (peak load or limit load), when the competition between the elastic restoring force of the fiber is overcome by the action of the external compressive load that deflects the fiber into a progressively deteriorating (in shear) matrix. Beyond this limit load, there can be ‘snap-back’ (both the macroscopic stress, σ , and the macroscopic axial strain, ϵ can decrease), resulting in an unstable equilibrium path. In the context of a laboratory experiment, the snap-back can be interpreted as a drop in stress instantaneously (at fixed ϵ) to the curving back path of the $\sigma - \epsilon$ curve (see dashed line in figure 8).

The carbon fiber composite response curves were first generated with isotropic properties of carbon fiber. For the case corresponding to the maximum value of misalignment, the properties of carbon fiber were changed to reflect material orthotropy and the compressive response was obtained. As can be seen from the results in Figure 8, the maximum stress is unaffected by fiber orthotropy but the post peak response is much softer in case of orthotropic fiber properties. The initial stiffness predicted by the 3D finite element model is nearly same for all the models with different imperfections, thus, establishing the “smallness” of the range of imperfection magnitudes selected for study.

In figure 9, the compressive response of the FE model with a misalignment angle of $\phi_1 = 1^\circ$ is shown. The response can be divided into three regions; the first is the pre-peak region where the response is linear, next, a post-peak region where the decrease in stress is very rapid, and, finally, a stage referred to as the plateau region where the stress is approaching a near constant value. Corresponding to the peak and post-peak regions, the displaced shape of the FE mesh has been plotted in figure 10. The meshes corresponding to step-4 lie near the peak and in the post-peak region of the curve. It can be seen that the deformation gradually increases as the stress starts to decrease beyond the peak stress value. As explained previously, the matrix starts to yield in shear at locations of maximum fiber misalignment thus causing a narrow band of fibers to rotate and propagate seemingly with no resistance, causing the macroscopic stress to drop. In the post-peak region, the mesh starts to show the formation of a distinct kink band and this distinction becomes clear as can be seen in the deformed mesh

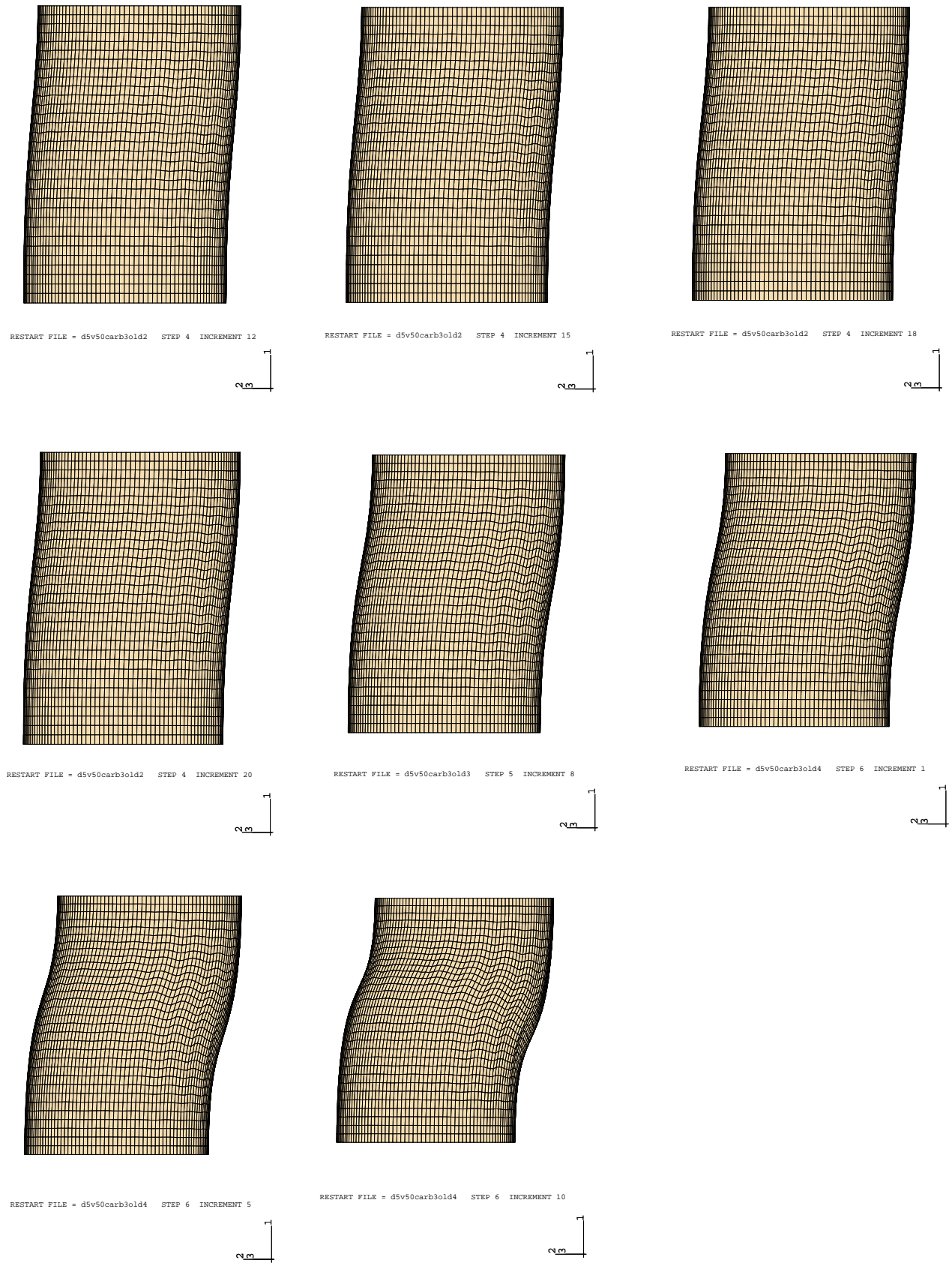


Figure 10 : Deformed mesh of carbon/vinylester composite of $V_f = 0.5$ and $\phi_1 = 1^0$ with orthotropic fiber properties

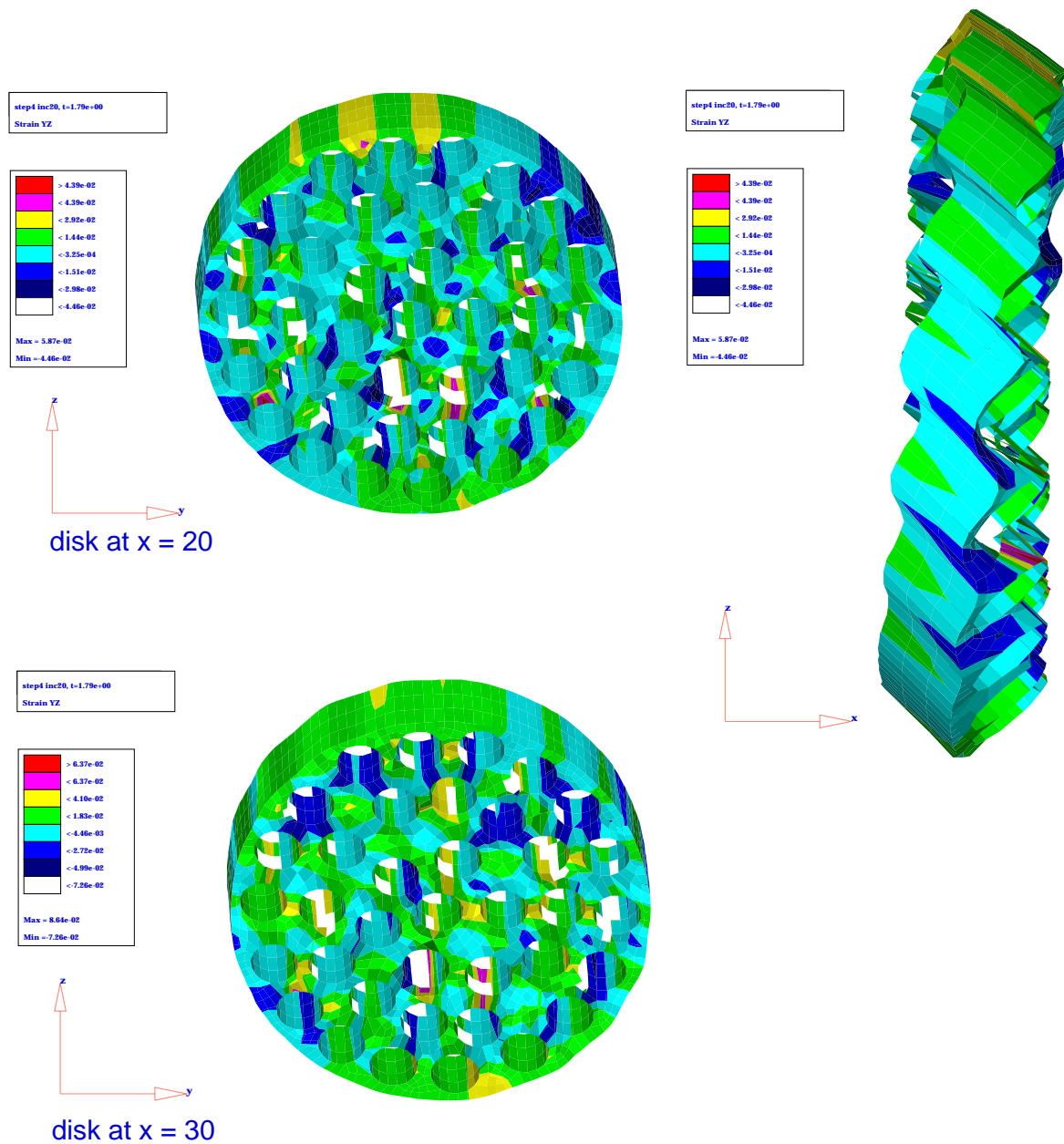


Figure 11 : Deformed mesh of a slice of the carbon/vinylester composite of $V_f = 0.5$ and $\phi_1 = 1^0$ with orthotropic fiber properties

corresponding to step-6. The stress corresponding to the deformed mesh for step-6, increment 10 is shown in the stress response curve and it can be seen that the point lies in the plateau region. An important observation that can be made from this 3D finite element simulation of kinking is the formation of circumferential ripples of increasing magnitude on the outer surface of the micro-section cylinder with continued loading, indicative of matrix regions which undergo shearing strains of differ-

ent sense (positive and negative shear). Unlike 2D simulation of kink bands where the matrix material within the kink band shows shearing of one sense (positive or negative), the outer surface of the composite in the 3D case shows ‘ripples’ which is reflected in the zig-zag nature of the deformed mesh in the kinked region. In fact as will be seen in figure 11, the circular shape of the composite no longer remains circular. In these figures, a slice of the composite without the embedded fibers is

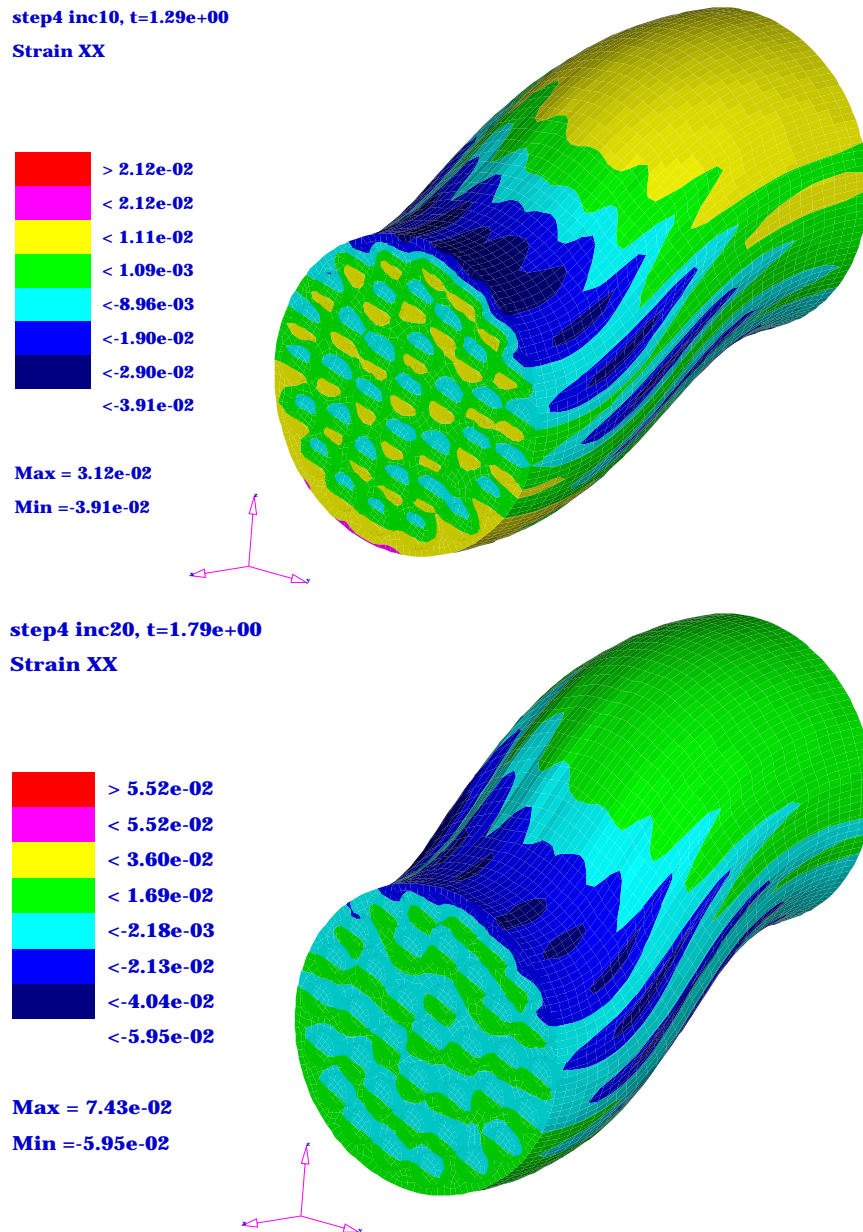


Figure 12 : Contours of ϵ_{xx} for the carbon/vinylester composite of $V_f = 0.5$ and $\phi_1 = 1^0$ with orthotropic fiber properties

shown. Figure 11 corresponds to the post-peak region of the compressive stress response curve. The side view of the deformed cross-section shows the ripples. On the deformed mesh, contours of inplane shear strain, γ_{yz} are superposed. The value of γ_{yz} increases as the post-peak region is reached. This also corresponds to the fact that the shape of the circular section no longer remains circular because of the inplane shear strains that develop. Contours of the uni-axial strain, ϵ_{xx} , are presented in figure

12. The strain contours are superposed on a deformed mesh. It was observed that, in the pre-peak region (step-1) the total strains are low, even though, one could notice the formation of a band of high strain region starting from one end of the composite and spreading diagonally across the surface. In the post-peak region (step-4) the strains started to increase and the strain localization initiated along the previously mentioned band indicated by the dark region in the strain contours (Figure 12). As the

post-peak region was approached, the band of high strain region started to grow and spread. The value of the peak strain in the band also increased. The region with elevated strain corresponded to the region of localized deformation of the mesh as seen in figure 10. A longitudinal section of the FE model for the carbon composite (with only the fibers) is presented in figure 13. The axial shear strain contours, γ_{xz} , are superposed over the deformed mesh. This is of interest in case of orthotropic fibers (like carbon), where the fiber itself has a microstructure. High values of inplane shear strain can cause the fiber to fail by shearing between outer layers and the fiber core (eg. in a onion skin core type of structure, [Herakovich (1998)]).

The procedure described for the 3D finite element simulation was also used to generate a perturbed mesh and obtain the compressive response of carbon fiber composite in a 2D plane strain setting. The comparison between the predicted maximum stress values for a 2D model and a 3D model are given in Table 6. As can be seen, the 3D model predictions are significantly lower at the same angle of initial fiber misalignment as compared to the 2D model predictions. Furthermore, the 3D model predictions are also lower than the analytical Budiansky-Fleck model predictions given by,

$$\sigma_c = \frac{\tau_y}{\phi + \gamma_y} \quad (1)$$

where τ_y is the shear yield stress of the composite, γ_y is the corresponding shear yield strain, and ϕ is the initial fiber misalignment angle.

	σ_c (MPa)	ϕ
Carbon-3D	495	2.3 ⁰
Carbon-2D	581	2.3 ⁰
BF-model	652	2.3 ⁰

Table 6 : Comparison of compressive strength predictions

3.2 Size Effects - Effect of fiber diameter

The 3D finite element micromechanical model of the glass fiber composite was used to study the effect of

fiber diameter on the peak stress under axial compression loading. For this purpose, two types of models were developed; one is referred to as a micro-mechanically scaled model and the other is referred to as a structurally scaled model. In the micro-mechanically scaled models, the FE models for both fiber diameters contained the same number of fibers and had similar fiber volume fractions. Thus, the outer radius of the FE model was different. In the case of structurally scaled models, the outer radius of both FE models and the fiber volume fraction were kept the same. This requires that the number of fibers in both models be different. In the case of the FE model with small fiber diameter, the number of fibers were taken to be 37 and in the case of the FE model with large fiber diameter, the number of fibers were taken to be 19. In passing, we note the extensive literature [Bazant, Kim, Daniel, Becq-Giraudon, and Zi (1999)] on the effect of structure size on the nominal compression strength of unidirectional fiber polymer composites.

3.2.1 Micro-mechanically Scaled Models

The shear stress-shear strain response from both models were found to be nearly same (Figure 14). Thus, an equivalence was established between the two micromechanically scaled FE models. Recall that the two glass composite models contain 37 fibers packed in a cylinder such that the overall fiber volume fraction, $V_f = 0.5$. The dimensions of the models are given in Table 1. The 3D models were next used to generate the compressive stress-compressive strain response. For the larger diameter fibers, the initial fiber misalignment values were varied. However, for comparing with the small fiber diameter model, two FE models with same value of initial misalignment were studied. From the response curves in figure 15, it can be seen that the peak stress in the case of the large fiber diameter model is high compared to the model with the small fiber diameter (at the same initial angle of misalignment). The analytical kinking stress prediction of [Budiansky and Fleck (1993)] (see equation (1)) would predict the peak stress to be the same for both cases since the composite shear stress-shear strain response is same for both models. However, as can be seen from the present FE model results, the peak stress is different with different reinforcing fiber diameters. This indicates that fiber bending stiffness plays an important role in the determination of the peak stress associated with kink banding. This novel result has not

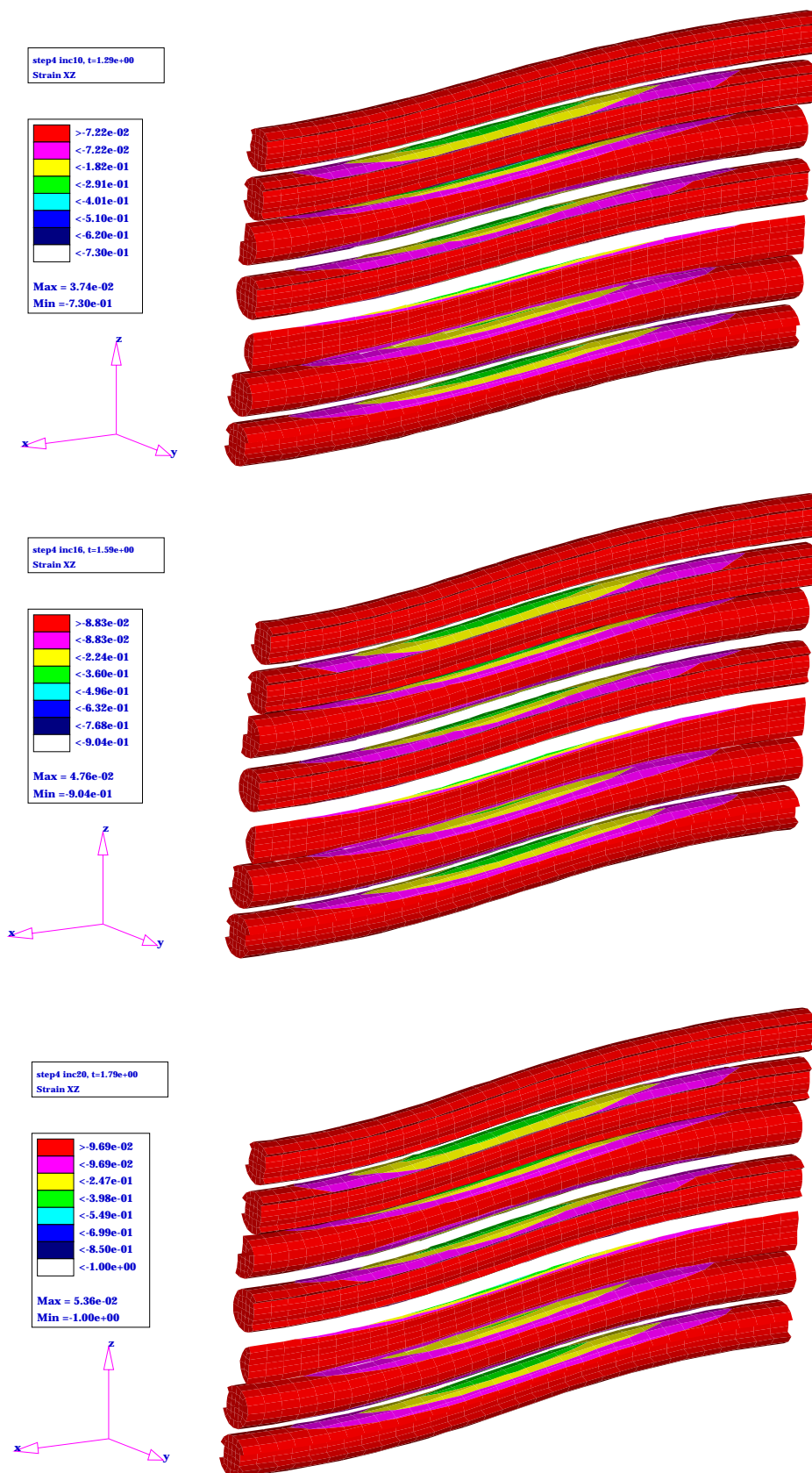


Figure 13 : Contours of γ_{xz} for the carbon/vinylester composite of $V_f = 0.5$ and $\phi_1 = 1^0$ with orthotropic fiber properties

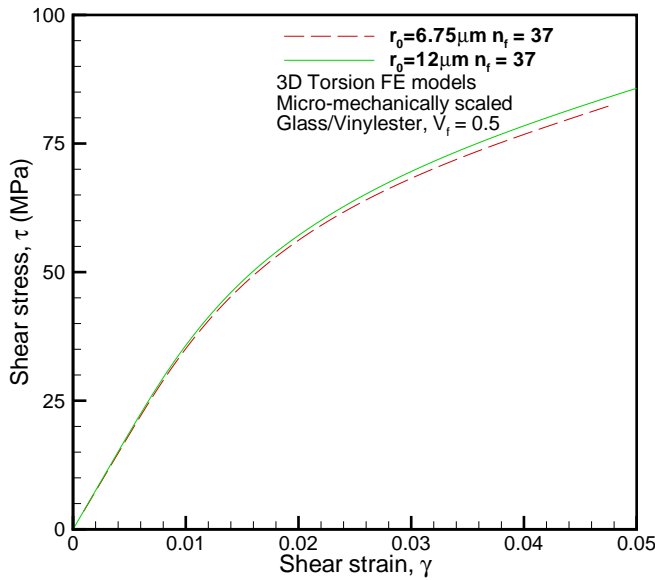


Figure 14 : Torsional response of a 3D FE model of a glass composite of $V_f = 0.5$ for micro-mechanically scaled models

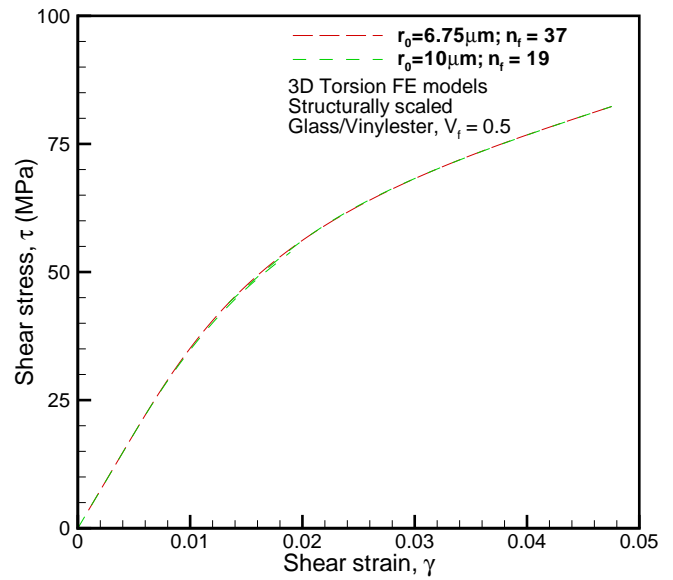


Figure 16 : Torsional response of a 3D FE model of a glass composite of $V_f = 0.5$ for structurally scaled models

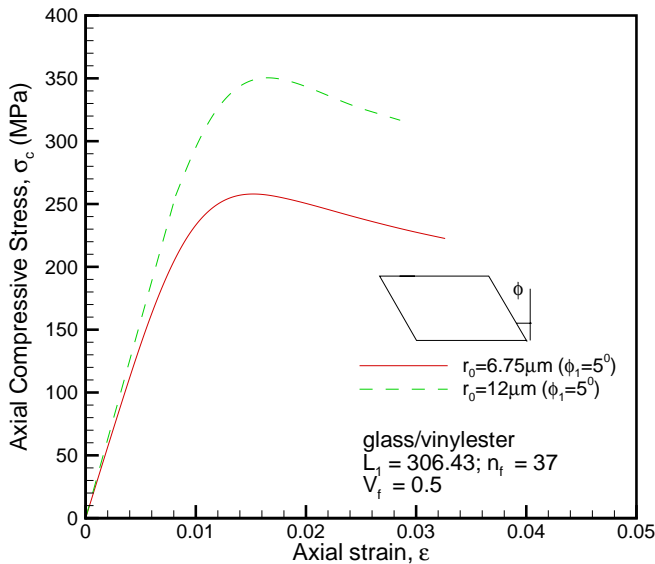


Figure 15 : Compressive stress response of a 3D FE model of a glass composite of $V_f = 0.5$ for micro-mechanically scaled models - effect of fiber diameter.

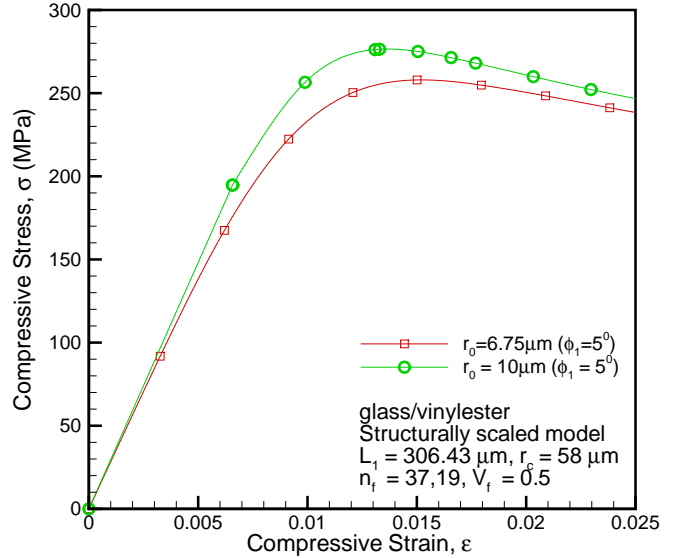


Figure 17 : Compressive stress response of a 3D FE model of a glass composite of $V_f = 0.5$ for structurally scaled models

been identified in previous 2D FE studies of kink banding (see [Vogler, Hsu, and Kyriakides (2001), Lee and Waas (1999)]). It should be noted that the analytical model for kinking by [Budiansky and Fleck (1993)] does not take into account the finite fiber bending stiffness and the extensibility of the fibers.

3.2.2 Structurally Scaled Model

Structurally scaled FE models were first subjected to pure torsion as was the case with the micromechanically scaled models, and the properties of the matrix material were ‘calibrated’ in order to obtain a similar macroscopic shear stress-shear strain response for both models with

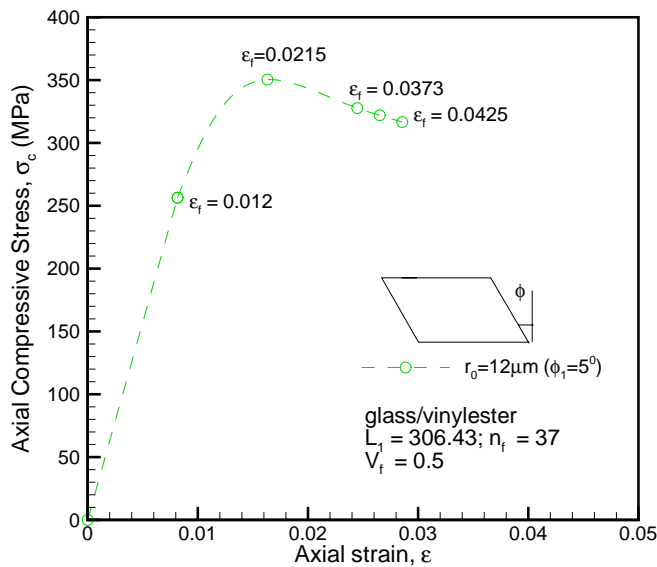


Figure 18 : Compressive stress response of a 3D FE model of a glass composite of $V_f = 0.5$ and $r_f = 12\mu\text{m}$

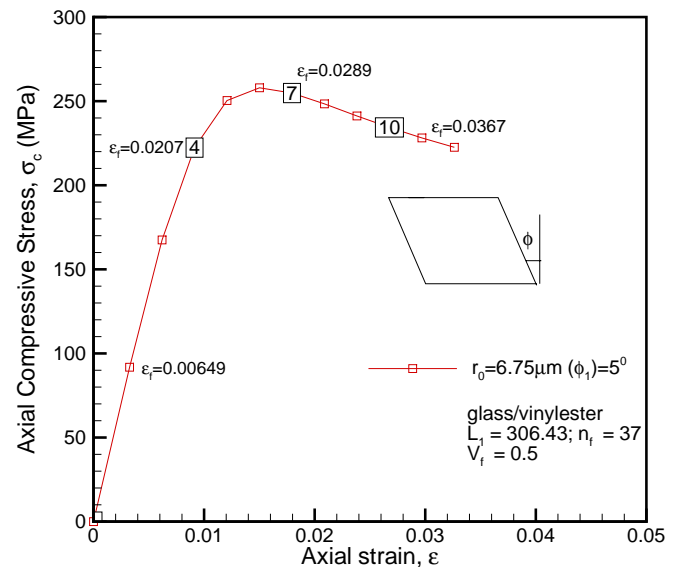


Figure 19 : Compressive stress response of a 3D FE model of a glass composite of $V_f = 0.5$ and $r_f = 6.75\mu\text{m}$

different diameter fibers as shown in figure 16. After this equivalence was established, the compressive response of the FE models were studied to understand the effect of fiber diameter on the peak compressive load. For comparison purposes, the initial fiber misalignment was kept the same for both FE models. As shown in figure 17, the peak compressive stress is different for both models and the model with a larger fiber diameter has a higher peak compressive stress for the same angle of misalignment. Thus, it is clear from both the structurally and the micro-mechanically scaled models that the fiber diameter does influence the peak compressive stress. The tendency is for the peak **compressive kinking** stress to increase with fiber diameter. The increase in composite compressive strength with increase in fiber diameter, as has been shown here, has been observed experimentally by [Schutz (1994)] for boron fiber composites, and by [Yerramalli (2003); Yerramalli and Waas (2003)] for glass fiber composites at low fiber volume fractions. However, it was also observed by [Yerramalli (2003)] that change in fiber diameter led to a change in the observed failure mechanism from kinking for small diameter fiber to splitting in case of large diameter glass fiber composites. Therefore, an increase in fiber diameter could lead to a different failure mechanism, thus limiting an increase to be gained in kinking compressive strength.

The micromechanically scaled FE model results are

shown in figure 18 and figure 19, where the maximum fiber strains are noted. It can be seen that for the same macroscopic axial strain, the local fiber strain is higher in the small fiber diameter FE model, compared against the larger diameter FE model. Furthermore, in this case (small fiber diameter), the maximum fiber strain is reached prior to the attainment of a maximum macroscopic load. This indicates the possibility of fiber breaking as the mechanism for initiation of failure, leading to kinking, in the case of small fiber diameter glass composite. In case of large diameter glass fibers, there are two possibilities. The fiber breaking strain is reached before or after the localized kink banding instability corresponding to a peak load. In the current study, assuming a fiber breaking strain of 0.02 for glass, it can be seen that, in the large fiber diameter model, the maximum fiber strain exceeds the fiber breaking strain almost at the maximum load point in the stress response curve. However, for the small fiber diameter model, the maximum fiber strain exceeds the fiber breaking strain much below the attainment of the maximum stress. Thus, the formation of kink bands, much like what has been experimentally observed by [Narayanan and Schadler (1999)] and [Garland, Beyerlein, and Schadler (2001)], can occur due to damage zones formed on account of fiber breaks prior to the attainment of a maximum load associated with a kink banding instability predicated on models that do not ac-

count for finite fiber bending stiffness. This finding is important, since it shows that the onset of kink banding and the associated kink band angle can be dependent on the fiber diameter and the fiber breaking strain when kink banding initiates from damage zones formed by fiber breaks. The fiber breaking strain is not a quantity that can be obtained from simple tension tests in general. For example, in case of carbon fibers that have a microstructure, the breaking strain under bending (with through thickness gradient loading) is different than the breaking strain in tension (where there is no through the thickness gradient in loading). These aspects have been pointed out by [Wisnom, Atkinson, and Jones (1997), Drapier, Grandidier, and Potier-Ferry (1999, 2001) and Quek (2002)].

4 Conclusions

In this paper, the results from a 3D finite element based micromechanics study on the kinking failure of unidirectional fiber composites have been presented. It can be seen that the fiber diameter and thus the finite fiber bending stiffness plays an important role in the determination of the compressive strength of FRPC. The results clearly indicate that kinking initiating due to a fiber break cannot be ignored in the case of small fiber diameter fiber composites. The quantitative results presented in this paper can be used to explain the microscopic experimental observations (based on Raman spectroscopy to track fiber breaks, as has been reported by [Narayanan and Schadler (1999) and Garland, Beyerlein, and Schadler (2001)]) on the initiation of kink bands. The 3D finite element simulation results show the importance of finite fiber bending stiffness on the compressive strength and the presence of a complex three dimensional stress state in the matrix region. Both of these effects are unaccounted for in previous models of kink banding that consider 2D models under plane strain condition. Based on 2D models the role of fiber misalignment on kink banding has previously been identified. The present results, on the other hand, show that other effects, controlled by fiber breaking strain and the fiber bending stiffness also effect composite compressive strength in a significant manner.

Acknowledgement: The authors are grateful to the Army Research Office for supporting this research. Dr. Bruce LaMattina is the ARO scientific monitor.

References

- Bazant, Z.; Kim, J.; Daniel, I.; Becq-Giraudon, E.; Zi, G.** (1999): Size effect on compression strength of fiber composites failing by kink band propagation. *International Journal of Fracture* 95, 103–141.
- Budiansky, B.; Fleck, N. A.** (1993): Compressive failure of fibre composites. *Journal of the Mechanics and Physics of Solids* 41 (1), 183–211.
- Drapier, S.; Grandidier, J.-C.; Potier-Ferry, M.** (1999): Towards a numerical model of the compressive strength for long fiber composites. *European Journal of Mechanics, A/Solids* 18 (1), 69–92.
- Drapier, S.; Grandidier, J.-C.; Potier-Ferry, M.** (2001): A structural approach of plastic microbuckling in long fibre composites: Comparison with theoretical and experimental results. *International Journal of Solids and Structures* 38 (22-23), 3877–3904.
- Fleck, N. A.** (1997): Compressive failure of fiber composites. In: *Advances in applied mechanics*. Vol. 33. Academic Press, New York, pp. 43–117.
- Garland, B. D.; Beyerlein, I. J.; Schadler, L. S.** (2001): Development of compression damage zones in fibrous composites. *Composites Science and Technology* 61 (16), 2461–2480.
- Herakovich, C. T.** (1998): *Mechanics of Fibrous Composites*. John Wiley and Sons.
- Iura, M.; Atluri, S. N.** (2003): Advances in finite rotations in structural mechanics. *CMES: Computer Modeling in Engineering & Sciences* 4 (2), 213–216.
- Jensen, H.** (1999): Analysis of compressive failure of layered materials by kink band broadening. *International Journal of Solids and Structures* 36 (23), 3427–3441.
- Kawabata, S.** (1988): *Measurements of Anisotropic Mechanical Property and Thermal Conductivity of Single Fiber for Several High Performance Fibers*. Technomic Press, Philadelphia, USA.
- Lee, S. H.; Waas, A. M.** (1999): Compressive response and failure of fiber reinforced unidirectional composites. *International Journal of Fracture* 100, 275–306.
- Mendelson, A.** (1983): *Plasticity: Theory and Application*. Krieger Publishing Company, Malabar, Florida.
- Naik, N. K.; Kumar, R. S.** (1999): Compressive strength of unidirectional composites: evaluation and comparison of prediction models. *Composite structures* 46, 299–308.

- Narayanan, S.; Schadler, L. S.** (1999): Mechanisms of kink-band formation in graphite/epoxy composites: a micromechanical experimental study. *Composite Science and Technology* 59, 2201–2213.
- Niu, K.; Talreja, R.** (2000): Modeling of compressive failure in fiber reinforced composites. *Int. J. of Solids and Structures* 37, 2405–2428.
- Pichler, B.; Mang, H. A.** (2000): New insights in nonlinear static stability analysis by the fem. *CMES: Computer Modeling in Engineering & Sciences* 1 (3), 43–55.
- Quek, S. C.** (2002): Compressive response and failure of braided textile composites : experiments and analysis. Ph.D. thesis, University of Michigan, Ann Arbor, MI.
- Schutz, J. B.** (1994): Properties of composite materials for cryogenic applications. *Cryogenics* 38 (1), 3–12.
- Vogler, T. J.; Hsu, S. Y.; Kyriakides, S.** (2000): Composite failure under combined compression and shear. *International Journal of Solids and Structures* 37, 1765–1791.
- Vogler, T. J.; Hsu, S. Y.; Kyriakides, S.** (2001): On the initiation and growth of kink bands in fiber composites. part II: analysis. *International Journal of Solids and Structures* 38, 2653–2682.
- Vogler, T. J.; Kyriakides, S.** (1999): Inelastic behavior of an as4/peek composite under combined transverse compression and shear. part I: experiments. *International Journal of Plasticity* 15, 783–806.
- Vogler, T. J.; Kyriakides, S.** (2001): On the initiation and growth of kink bands in fiber composites. part I: experiments. *International Journal of Solids and Structures* 38, 2639–2651.
- Waas, A. M.; Schultheisz, C. R.** (1996): Compressive failure of composites parts I and II. *Progress in Aerospace Sciences* 32 (1), 1–78.
- Wisnom, M. R.; Atkinson, J. W.; Jones, M. I.** (1997): Reduction in compressive strain to failure with increasing specimen size in pin-ended buckling tests. *Composites Science and Technology* 57 (9-10), 1303–1308.
- Yerramalli, C. S.** (2003): A mechanism based modeling approach to failure in fiber reinforced composites. Ph.D. thesis, Aerospace Engineering Department, University of Michigan, Ann Arbor.
- Yerramalli, C. S.; Waas, A. M.** (2003): A new failure criterion for fiber reinforced polymer composites under combined compression-torsion loading. *International Journal of Solids and Structures* 40, 1139–1164.